PHYSICAL REVIEW B VOLUME 48, NUMBER 17 1 NOVEMBER 1993-I

Fluctuation conductivity of layered superconductors in a perpendicular magnetic field

V. V. Dorin, R. A. Klemm, and A. A. Varlamov
Materials Science Division, Argonne National Laboratory, 9700 South Cass Avenue, Argonne, Illinois 60439

A. I. Buzdin
Institute for High Pressure Physics, Academy of Sciences of Russia, Troitsk 142092, Russia
and Materials Science Division, Argonne National Laboratory, 9700 South Cass Avenue, Argonne, Illinois 60439

D. V. Livanov
Moscow Institute of Steel and Alloys, Leninskiĭ Prospect 4, Moscow 117936, Russia

(Received 14 June 1993; revised manuscript received 14 July 1993)

The leading contributions to the c-axis conductivity of layered superconductors arising from superconducting fluctuations of the order parameter are discussed for arbitrary intralayer scattering. The contributions from fluctuations of the normal quasiparticle density of states are shown to be opposite in sign to the Aslamazov-Larkin and Maki-Thompson contributions, leading to a peak in the overall c-axis resistivity $\rho_c(T)$ above T_c. This peak is enhanced by a magnetic field $\mathbf{H}\|\hat{\mathbf{c}}$. With increasing H, the relative peak maximum in $\rho_c(T,H)$ increases in magnitude and is shifted to lower temperatures by an amount proportional to H^2 for weak fields and to H for strong fields. For comparison, the fluctuation conductivity parallel to the layers has been calculated including the fluctuations of the normal density of states. Our results are discussed in regard to recent experiments with $YBa_2Cu_3O_{7-\delta}$ and $Bi_2Sr_2CaCu_2O_{8+\delta}$.

I. INTRODUCTION

One of the main characteristics of a superconductor is the temperature T dependence of the resistivity in the vicinity of the superconducting transition temperature T_c. In layered superconductors, the zero-field resistivity is a diagonal tensor, and care must be taken to extract the tensor components $\rho_{ii}(T)$ from the data obtained using various current and voltage configurations.[1] The first measurements of the anisotropic resistivity tensor in the vicinity of T_c in a layered superconductor were made on TaS_2 (pyridine)$_{1,2}$.[2] In this material, intercalation with pyridine suppressed the charge-density wave present in the unintercalated $2H$-TaS_2, as well as increased its anisotropy greatly. In addition, the c-axis resistivity element $\rho_{cc}(T)\equiv\rho_c(T)$ in some samples was found to increase with decreasing T, exhibiting a peak just above T_c, before falling rapidly to zero at T_c. This peak became more pronounced in a magnetic field $\mathbf{H}\|\hat{\mathbf{c}}$, with $\rho_c(T,H)$ continuing to rise with decreasing $T<T_c(0)$ before falling rapidly to zero as $T\rightarrow T_c(H)$. Such a peak was not observed in the in-plane resistivity $\rho_{ab}(T)$. Except for one theoretical paper,[3] this effect generated little interest at the time.

More recently, the resistivities of many high-T_c cuprates have been studied by numerous groups.[1,4–6] Although early measurements were usually made on ceramic samples or imperfect crystals, reliable results on untwinned samples of YBa2$Cu_3O_{7-\delta}$ (YBCO) (Refs. 4–6) and on $Bi_2Sr_2CaCu_2O_{8+\delta}$ (BSCCO) have since been presented.[1,7] Generally, it has been found that fully oxygenated YBCO appears metallic along all three crystal axis directions, although oxygen-deficient YBCO can exhibit a peak in $\rho_c(T)$.[8] The main difference between $\rho_c(T)$ and $\rho_{ab}(T)$ in fully oxygenated YBCO is that $\rho_{ab}(T)$ exhibits dimensional crossover from 2D to 3D at $T_0>T_c$, whereas $\rho_c(T)$ exhibits dimensional crossover from 0D to 3D at T_0.[3,6,9] In BSCCO, on the other hand, $\rho_c(T)$ reproducibly exhibits a peak, which increases in magnitude with decreasing oxygen concentration.[10] In addition, a rather weak magnetic field $\mathbf{H}\|\hat{\mathbf{c}}$ causes the relative magnitude of the peak to increase, and its position to shift dramatically to lower $T>T_c(H)$ values.[7]

Recently, it was proposed[9] that such a peak in $\rho_c(T)$ could arise from superconducting fluctuations, and the calculations[9] were found to be in agreement with experiments on epitaxially grown thin films of BSCCO.[10] The main idea of this explanation is that the positive contributions to the fluctuation conductivity in the c-axis direction are *weak* above T_0, arising from the hopping or tunneling nature of the single quasiparticle c-axis propagation. Hence, the less-singular contribution *of the opposite sign* to the conductivity arising from the fluctuation decrease of the single quasiparticle density of states (DOS) at the Fermi energy ϵ_F becomes dominant above T_0. The competition between these contributions gives rise to the peak, or maximum in $\rho_c(T)$ just above T_c. In some circumstances, the Maki-Thompson (MT) diagrams can be relevant, but such contributions were omitted in that treatment,[9] as the assumption of strong pair breaking was made.

Nevertheless, the question of the strong increase of the magnitude of this peak and its shift to lower temperatures in a magnetic field was not addressed in the above treatment.[9] Some ideas were proposed as possible ex-

©1993 The American Physical Society

planations for this effect, most of them depending upon some revision of the theory of the fluctuation conductivity to account for the broadening of the resistive transition in the high-T_c superconductors in a magnetic field.[11,12] In these papers, the effect of the magnetic field upon the superconducting fluctuations of the order parameter was treated in a self-consistent way, removing the divergence of the fluctuation conductivity at the mean-field $T_c(H)$. We will not discuss the validity of such approximations, except to note that just below the mean-field $T_c(H)$, the structure of the fluctuation propagator is considerably more complicated[13] than assumed by those authors.[11] However, all such papers used the time-dependent Ginzburg-Landau (TDGL) or equivalent approximations to the paraconductivity, treating the magnetic-field dependence of $T_c(H)$ in some self-consistent approximation. None of these papers considered the effect of the fluctuation corrections to the quasiparticle density of states,[9] which occurs in the same (first) order in the fluctuation propagator[14,15] as do the contributions leading to the TDGL approximation. Hence, such treatments *cannot* explain the peak in $\rho_c(T)$. Furthermore, the MT contributions were ignored in all such treatments.

Very recently, a phenomenological model of the c-axis conduction in highly anisotropic layered materials has been proposed,[16] and found to account for the peak in $\rho_c(T,H)$ observed in BSCCO. In this model, there is a competition between the decrease in the quasiparticle current density with decreasing temperature and the increase in the interlayer currents due to the appearance of Josephson-like shorts in a magnetic field below T_c. With respect to the increase in the resistance with decreasing temperature above T_c, this model has the same physical origin as in Ref. 9. However, the decrease in the resistivity below the peak was attributed to different mechanisms in Refs. 9 and 16. In Ref. 9, the zero-field decrease above T_c was attributed to paraconductivity. On the other hand, in Ref. 16, the magnetic field itself was responsible for the increase in the interlayer Josephson coupling.

In this work, we have studied the leading contributions to $\rho_c(T,H)$ arising from superconducting fluctuations of the order parameter in the presence of a perpendicular magnetic field $\mathbf{H}\|\hat{\mathbf{c}}$. In Sec. II, we review the existing zero-field results for the various contributions,[3,6,9,15,17,18] examine the MT contributions in detail, and discuss possible higher-order contributions. All contributions are evaluated for arbitrary intralayer impurity scattering. In Sec. III, we consider the effect of a perpendicular magnetic field upon these contributions, using existing results[3] for the Aslamazov-Larkin (AL) diagram, and evaluating analytically the remaining contributions to the extent possible. As mentioned above, we shall show that the peak in $\rho_c(T,H)$ increases with increasing H, and shifts to lower T values. In Sec. IV, results for the fluctuation conductivity parallel to the layers are given, including the DOS contribution, which has always been neglected previously, but which is relevant for rather clean materials. In Sec. V, we summarize and discuss our results, comparing them with recent experiments on YBCO and BSCCO. We use units in which $\hbar=k_B=c=1$.

II. ZERO-FIELD RESULTS

A. The model

We begin by discussing the quasiparticle normal-state energy spectrum. While models with several conducting layers per unit cell and with either intralayer or interlayer pairing have been considered,[19] it has recently been shown[20] that all of these models give rise to a Josephson pair potential that is periodic in k_z, the wave vector component parallel to the c axis, with period s, the c-axis repeat distance. While such models give rise to distinct differences in the superconducting densities of states, they all give rise to qualitatively similar fluctuation propagators, which differ only in the precise definitions of the parameters and in the precise form of the Josephson coupling potential.[20] Ignoring the rather unimportant differences between such models in the Gaussian fluctuation regime above $T_c(H)$, we therefore consider the simplest model of a layered superconductor, in which there is one layer per unit cell, with intralayer singlet s-wave pairing,[3,21]

$$\xi(p)=\epsilon_0(\mathbf{p})+J\cos(p_z s)-E_F\ , \tag{1}$$

where $\epsilon_0(\mathbf{p})=\mathbf{p}^2/(2m)$, $p\equiv(\mathbf{p},p_z)$, $\mathbf{p}\equiv(p_x,p_y)$ is a two-dimensional, intralayer wave vector, and J is an effective quasiparticle nearest-neighbor interlayer hopping energy. The Fermi surface defined by $\xi(p_F)=0$ is a corrugated cylinder, and E_F is the Fermi energy. As described previously,[21] this model is most appropriate for highly anisotropic layered materials, for which $J/E_F \ll 1$.

We remark that the paraconductivity obtained in zero field in this model has a leading contribution above T_0 of second order in the interlayer pair transmittance ($\propto J^4$).[3,6,9] In this regime, tunneling processes in which the quasiparticles can propagate to next-nearest-neighbor layers with probability proportional to J^2 would be of comparable magnitude.[22] Such processes can be included by adding a correction to (1) of the form $J_2\cos(2p_z s)$, where $J_2 \propto J^2$. However, it turns out that such processes give rise to a paraconductivity above T_0 of second order in the pair transmittance of this higher-order process (i.e., $\propto J_2^4 \propto J^8$) due to the orthogonality of the $\cos(p_z s)$ and $\cos(2p_z s)$ wave functions, and can therefore be neglected.

In addition, some remark regarding the normal-state quasiparticle momentum relaxation time is in order. In the "old" layered superconductors such as TaS_2 (pyridine)$_{1/2}$, the materials were generally assumed to be in the dirty limit.[21] In the high-T_c cuprates, however, both single crystals and epitaxial thin films are nominally in the "clean" limit, with l/ξ_{ab} values generally exceeding unity, where l and ξ_{ab} are the intralayer mean-free path and BCS coherence length, respectively. However, as $l/\xi_{ab}\approx 2-5$ for most of the cuprates, these materials are not extremely clean. In addition, the situation in the cuprates is complicated by the presence of phonons for $T\simeq T_c\simeq 100$ K, the nearly localized magnetic moments on the Cu^{2+} sites, and by other unspecified inelastic processes. Experiments on high-T_c cuprates have shown that the excess "in-plane" conductivity can usually be explained in terms of the fluctuation paraconductivity alone.[23]

Finally, magnetoresistance measurements in $YBa_2Cu_3O_{7-\delta}$ have been interpreted[24,25] as giving an extremely small value of the phase pair-breaking lifetime $\tau_\phi \approx 1/T$. We note, however, that such an interpretation was based upon the extraction of τ_ϕ from the fluctuation conductivity for $\mathbf{H}\perp\hat{\mathbf{c}}$, for which it was assumed that the orbital pair breaking could be neglected, leaving the Pauli (or Zeeman) contribution to the MT diagram as the leading contribution to $\sigma_{xx}^{\mathrm{MT}}$.[24,25] As will be shown elsewhere,[26] such an extraction is suspect, as the procedure followed does not give the correct result for the upper critical field parallel to a thin film or to the layers in a layered superconductor,[21] which in both cases is dominated by orbital pair breaking for weak fields ($H \ll 100$ T), and Pauli pair breaking *only* for fields comparable to $H_p = 1.86(\mathrm{T/K})T_c \approx 150$ T. Hence, it is possible that the true τ_ϕ could be much larger than inferred in either of those fits.[24,25]

In the following, we assume simple elastic intralayer scattering,[21] keeping the impurity concentration n_i and the resulting scattering rate $1/\tau$ arbitrary, and allowing for an arbitrary phase pair-breaking rate $1/\tau_\phi < 1/\tau$.

We now consider the various diagrams for the electromagnetic response operator $Q_{\alpha\beta}(\omega_\nu)$, which may contribute to the c-axis fluctuation conductivity of layered superconductors. Some of these diagrams are presented in Fig. 1. In this notation, the subscripts α and β refer to polarization directions and thus to the conductivity tensor elements, and the $\omega_\nu = (2\nu+1)\pi T$ are the Matsubara frequencies. Intralayer quasiparticle scattering is included in the Born approximation, giving rise to a scattering lifetime τ and resulting in a renormalization of the single quasiparticle normal-state Green's function to[21]

$$G(p,\omega_n) = \frac{1}{i\tilde{\omega}_n - \xi(p)} , \tag{2}$$

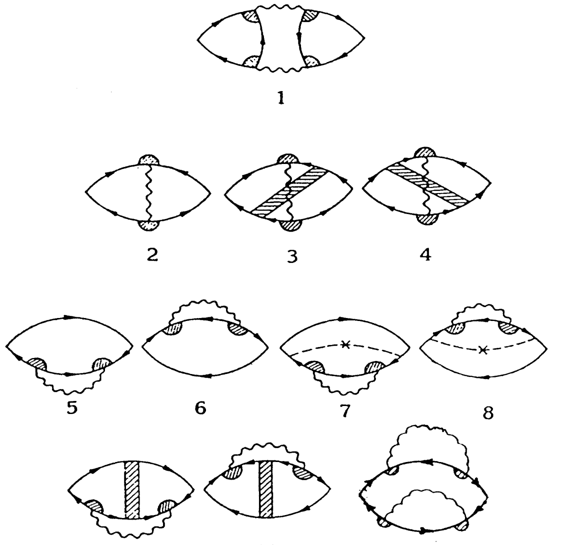

FIG. 1. Shown are the leading Feynman diagrams for the fluctuation conductivity. Wavy lines are fluctuation propagators, thin solid lines with arrows are impurity-averages normal-state Green's functions (2). Shaded partial circles are vertex corrections arising from impurities, dashed curves with central crosses are additional impurity renormalizations, and shaded thick lines are additional impurity vertex corrections. Diagram 1 is the Aslamazov-Larkin diagram, diagrams 3–5 are Maki-Thompson diagrams, and diagrams 5–10 are the leading diagrams giving corrections to the normal density of states. Diagram 11 is a higher-order correction to the density of states.

where

$$\tilde{\omega}_n = \omega_n[1 + 1/(2|\omega_n|\tau)] .$$

Such renormalizations are indicated in the vertices of Fig. 1 by shadowing. The resulting expression for the triangle vertex, valid for arbitrary impurity concentration n_i, is[27]

$$C(q,\omega_n,\omega_{n'}) = \left[1 - \frac{\Theta(-\omega_n\omega_{n'})}{\tau(\tilde{\omega}_n - \tilde{\omega}_{n'})} \left[1 - \frac{\langle [\xi(p)-\xi(q-p)]^2 \rangle}{(\tilde{\omega}_n - \tilde{\omega}_{n'})^2} \right] \right]^{-1} , \tag{3}$$

where $\Theta(x)$ is the Heaviside step function, and $\langle \cdots \rangle$ denotes an average over the Fermi surface. Performing the Fermi surface average, we find

$$\langle [\xi(p)-\xi(q-p)]^2 \rangle = \tfrac{1}{2}[v_F^2 \mathbf{q}^2 + 4J^2 \sin^2(q_z s/2)] \equiv \tau^{-1} D\hat{Q}^2 , \tag{4}$$

where $v_F = |\mathbf{p}_F|/m$ is the magnitude of the Fermi velocity parallel to the layers. In (3), we have made the assumption $\tau D\hat{Q}^2 \ll 1$, which we make throughout this manuscript. Hence, we neglect nonlocal corrections. This approximation is described in detail in Sec. V.

With each external entrance to the diagrams of the electromagnetic field component α with electromagnetic coupling eA_α, we associate the external vertex $ev_\alpha(p)$, where e is the quasiparticle electronic charge, and

$$v_\alpha(p) = \frac{\partial \xi(p)}{\partial p_\alpha} .$$

For longitudinal conductivity tensor elements (parallel to the layers, for which $\alpha = x,y$), the resulting vertex is simply ep_α/m. For the c-axis conductivity, the vertex $ev_z(p)$ is obtained from [3]

$$v_z(p) = \frac{\partial \xi(p)}{\partial p_z} = -Js\sin(p_z s) . \tag{5}$$

Each wavy line in the diagrams is a *fluctuation propagator* $L(q,\omega_\mu)$, which is a chain of superconducting bubble diagrams. We integrate over the internal momenta q

and sum over the internal Matsubara frequencies ω_μ, with momentum and energy conservation at each internal vertex (fluctuation propagator endpoint). At $H=0$ in the vicinity of T_c, the inverse of $L(q,\omega_\mu)$ has the form

$$L^{-1}(q,\omega_\mu)=-\rho\left[\epsilon+\psi\left[\frac{1}{2}+\frac{\omega_\mu}{4\pi T}+\alpha_q\right]-\psi\left[\frac{1}{2}\right]\right], \tag{6}$$

where

$$\epsilon=\ln(T/T_c)\approx(T-T_c)/T_c$$

for $T-T_c \ll T_c$, $\psi(x)$ is the digamma function, $\rho=N(0)=m/(2\pi s)$ is the single-spin quasiparticle normal density of states,

$$\alpha_q=\frac{4\eta D\hat{Q}^2}{\pi^2 v_F^2\tau}, \tag{7}$$

and

$$\eta=-\frac{v_F^2\tau^2}{2}\left[\psi\left[\frac{1}{2}+\frac{1}{4\pi\tau T}\right]-\psi\left[\frac{1}{2}\right]-\frac{1}{4\pi\tau T}\psi'\left[\frac{1}{2}\right]\right]$$
$$\to\frac{\pi v_F^2\tau}{16T}\begin{cases}1 & \text{for } \tau T\ll 1,\\ 7\zeta(3)/(2\pi^3\tau T) & \text{for } \tau T\gg 1\end{cases} \tag{8}$$

is the positive constant which enters into the current expression in the phenomenological GL theory in two dimensions,[28] where $\psi'(x)$ is the derivative of the digamma function and $\zeta(x)$ is the Riemann zeta function.

B. Aslamazov-Larkin contribution

We first examine the AL contribution $Q_{zz}^{\mathrm{AL}}(\omega_\nu)$ (diagram 1 of Fig. 1) to the c-axis fluctuation conductivity, where

$$Q_{\alpha\beta}^{\mathrm{AL}}(\omega_\nu)=2e^2T\sum_{\omega_\mu}\int\frac{d^3q}{(2\pi)^3}B_\alpha(q,\omega_\mu,\omega_\nu)L(q,\omega_\mu)\times L(q,\omega_\mu+\omega_\nu)B_\beta(q,\omega_\mu,\omega_\nu), \tag{9}$$

where

$$\int d^3q\equiv\int d^2\mathbf{q}\int_{-\pi/s}^{\pi/s}dq_z$$

is the appropriate integral for a layered superconductor,[3,6,9] and

$$B_\alpha(q,\omega_\mu,\omega_\nu)=T\sum_{\omega_n}\int\frac{d^3p}{(2\pi)^3}v_\alpha(p)C(q,\omega_{n+\nu},\omega_{\mu-n})C(q,\omega_n,\omega_{\mu-n})\times G(p,\omega_{n+\nu})G(p,\omega_n)G(q-p,\omega_{\mu-n}), \tag{10}$$

where $C(q,\omega_n,\omega_{n'})$ is given by (3), and $\omega_{n\pm\nu}=\omega_n\pm\omega_\nu$, etc. Since $v_z(p)$ is odd in p_z from (5), $B_z(q,\omega_\mu,\omega_\nu)$ is proportional to J^2 to leading order in J. In the vicinity of T_c, the leading contribution to the c-axis conductivity response Q_{zz}^{AL} arises from the fluctuation propagators in (9) rather than from the frequency dependences of the vertices B_z, so it suffices to neglect the ω_μ and ω_ν dependences of B_z. This approximation leads to

$$B_z(q)\approx-2\rho\frac{\eta}{v_F^2}sJ^2\sin(q_zs). \tag{11}$$

Using this expression in (9) followed by analytic continuation of the external Matsubara frequencies to the imaginary axis [to obtain the appropriate retarded response $Q^R(\omega)$] and integration over q_z, the zero-frequency AL contribution to the c-axis fluctuation conductivity was found in the static limit to be[3,6,9]

$$\sigma_{zz}^{\mathrm{AL}}=-\lim_{\omega\to 0}\frac{1}{i\omega}(Q_{zz}^{\mathrm{AL}})^R(\omega)$$
$$=\frac{\pi e^2sr^2}{32}\int\frac{d^2\mathbf{q}}{(2\pi)^2}\frac{1}{[(\eta\mathbf{q}^2+\epsilon)(\eta\mathbf{q}^2+\epsilon+r)]^{3/2}}$$
$$=\frac{e^2s}{32\eta}\left[\frac{\epsilon+r/2}{[\epsilon(\epsilon+r)]^{1/2}}-1\right]$$
$$\to\frac{e^2s}{64\eta}\begin{cases}(r/\epsilon)^{1/2}, & \text{for } \epsilon\ll r,\\ [r/(2\epsilon)]^2, & \text{for } \epsilon\gg r,\end{cases} \tag{12}$$

where

$$r=4\eta J^2/v_F^2$$
$$\to\frac{\pi J^2\tau}{4T}\begin{cases}1 & \text{for } \tau T\ll 1,\\ 7\zeta(3)/(2\pi^3\tau T)\approx 0.1357/(\tau T) & \text{for } \tau T\gg 1,\end{cases} \tag{13}$$

where $r(T_c)=4\xi_\perp^2(0)/s^2$ is the usual anisotropy parameter[3] characterizing the dimensional crossover from the 2D to the 3D regimes in the thermodynamic fluctuation behavior at T_0 (except for σ_{zz}, for which the crossover is from 0D to 3D at T_0), and $\xi_\perp(0)$ is the zero-temperature Ginzburg-Landau coherence length in the c-axis direction. Although dynamic corrections were found to be significant for the AL fluctuation conductivity parallel to the layers in the 2D regime above T_0,[29,30] such corrections to the c-axis fluctuation conductivity were found to be negligible, so (12) is accurate in the entire temperature range above T_c. We remark that with the expression (8) for η, both the clean ($4\pi\tau T_c\gg 1$) and dirty ($4\pi\tau T_c\ll 1$) limit results can be expressed using the same formulas, as in (12) above.

In the region $\xi_\perp(T)\ll s/2$ of two-dimensional fluctuation behavior, $\sigma_{zz}^{\mathrm{AL}}$ is suppressed from the static in-plane fluctuation conductivity $\sigma_{xx}^{\mathrm{AL}}$ by the factor

$$[2\xi_\perp(T)/s]^2(\sigma_{zz}^N/\sigma_{xx}^N),$$

so that the other contributions to the transverse fluctuation conductivity need to be considered as well. The normal-state conductivities in this model are

$$\sigma_{xx}^N=N(0)e^2v_F^2\tau/2=E_F\tau e^2/(2\pi s),$$

and $\sigma_{zz}^N/\sigma_{xx}^N = J^2 s^2/v_F^2$ is the square of the ratio of effective Fermi velocities in the parallel and perpendicular directions, respectively.

C. Contributions from fluctuations of the density of states

The specific forms of the AL and, as shown below, MT contributions to the fluctuation conductivity, which are suppressed for small interlayer transmittance, suggest that one should compare these terms with those arising from other, less divergent, diagrams which are of lower order in the transmittance.[9] Such diagrams are pictured in diagrams 5–10 of Fig. 1. These (DOS) diagrams arise from corrections to the normal quasiparticle density of states due to fluctuations of the normal quasiparticles into the superconducting state. In the dirty limit, the calculation of the contributions to the longitudinal fluctuation conductivity (σ_{xx}, parallel to the layers) from such diagrams was discussed previously.[31] Diagrams 9 and 10 arise from averaging diagrams 5 and 6 over impurity positions. It was shown[31] for the longitudinal fluctuation conductivity that diagrams 9 and 10 are less temperature dependent than diagrams 5 and 6, and can therefore be neglected. In the dirty limit, diagrams 7 and 8 were shown[31] to be equal to $-\frac{1}{3}$ times diagrams 5 and 6, which are evidently equal to each other. In the clean limit, diagrams 7 and 8 can be neglected relative to diagrams 5 and 6. For general impurity scattering, the ratio of these diagrams depends upon τ. It is easy to generalize those arguments to the case of the c-axis (transverse) fluctuation conductivity, by replacing the electromagnetic vertices $ev_\alpha(p)$ (which were approximated in Ref. 31 by ev_F) by the appropriate components $[ev_z(p)]$. As we are interested in the results for arbitrary impurity concentration, we shall evaluate these diagrams separately. The contribution to the c-axis fluctuation conductivity due to diagram 5 is

$$Q_{zz}^5(\omega_\nu) = 2e^2 T \sum_{\omega_\mu} \int \frac{d^3q}{(2\pi)^3} L(q,\omega_\mu) T \sum_{\omega_n} \int \frac{d^3p}{(2\pi)^3} v_z^2(p) C^2(q,\omega_n,\omega_{\mu-n}) G^2(p,\omega_n) G(q-p,\omega_{\mu-n}) G(p,\omega_{n+\nu}) , \tag{14}$$

and diagram 6 gives an identical contribution. Evaluation of the integrations over the internal momenta **p** and the summation over the internal frequencies ω_n are straightforward. Treatment of the other internal frequencies ω_μ is less obvious, but in order to obtain the leading singular behavior in $\epsilon \ll 1$ of Q_{zz}^5, it is possible to set $\omega_\mu = 0$. This point is nontrivial, as the same approximation in the AL diagram would lead to a result that would differ from the correct one (12) by a factor of 2. After integration over q_z, we have

$$\begin{aligned}
\sigma_{zz}^{5+6} &= -\frac{e^2 s \pi r_1}{4} \int_{|\mathbf{q}| \le q_{\max}} \frac{d^2\mathbf{q}}{(2\pi)^2} \frac{1}{[(\epsilon+\eta\mathbf{q}^2)(\epsilon+r+\eta\mathbf{q}^2)]^{1/2}} \\
&= -\frac{e^2 s r_1}{8\eta} \ln \left[\frac{(\epsilon+\eta q_{\max}^2)^{1/2} + (\epsilon+r+\eta q_{\max}^2)^{1/2}}{\epsilon^{1/2}+(\epsilon+r)^{1/2}} \right] \\
&\approx -\frac{e^2 s r_1}{8\eta} \ln \left[\frac{2}{\epsilon^{1/2}+(\epsilon+r)^{1/2}} \right] ,
\end{aligned} \tag{15}$$

where

$$r_1 = \frac{2(J\tau)^2}{\pi^2} \left[\psi' \left[\frac{1}{2} + \frac{1}{4\pi T\tau} \right] - \frac{3}{4\pi T\tau} \psi'' \left[\frac{1}{2} \right] \right] . \tag{16}$$

In the clean limit, (15) reduces to that obtained in Ref. 9. In (15), we have introduced a cutoff in the integral at $|\mathbf{q}| = q_{\max}$, where $\eta q_{\max}^2 \approx 1$, as in Refs. 9 and 10. This cutoff arises from the q dependence of the vertices and of the Green's function, which had been neglected in comparison with the contribution from the propagator, and is appropriate for both the clean and dirty limits.

In the similar manner, the equal contributions from diagrams 7 and 8 sum to

$$\begin{aligned}
\sigma_{zz}^{7+8} &= -\frac{e^2 s \pi r_2}{4} \\
&\times \int_{|\mathbf{q}| \le q_{\max}} \frac{d^2\mathbf{q}}{(2\pi)^2} \frac{1}{[(\epsilon+\eta\mathbf{q}^2)(\epsilon+r+\eta\mathbf{q}^2)]^{1/2}} \\
&\approx -\frac{e^2 s r_2}{8\eta} \ln \left[\frac{2}{\epsilon^{1/2}+(\epsilon+r)^{1/2}} \right] ,
\end{aligned} \tag{17}$$

where

$$r_2 = \frac{J^2\tau}{2\pi^3 T} \psi'' \left[\frac{1}{2} \right] . \tag{18}$$

Comparing (15) and (17), we see that in the clean limit the main contributions from the DOS fluctuations arise from diagrams 5 and 6. In the dirty limit, diagrams 7 and 8 are also important, having $-\frac{1}{3}$ the value of diagrams 5 and 6, as for σ_{xx}. Diagrams 9 and 10 are not singular in $\epsilon \ll 1$ in the 2D regime above T_0 and can be neglected. The total DOS contributions to the c-axis conductivity are therefore

$$\sigma_{zz}^{\rm DOS} = -\frac{e^2 s r}{8\eta} \kappa \ln \left[\frac{2}{\epsilon^{1/2}+(\epsilon+r)^{1/2}} \right] , \tag{19}$$

where

$$\kappa=\frac{r_1+r_2}{4}=\frac{-\psi'\left[\frac{1}{2}+\frac{1}{4\pi\tau T}\right]+\frac{1}{2\pi\tau T}\psi''\left[\frac{1}{2}\right]}{\pi^2\left[\psi\left[\frac{1}{2}+\frac{1}{4\pi\tau T}\right]-\psi\left[\frac{1}{2}\right]-\frac{1}{4\pi\tau T}\psi'\left[\frac{1}{2}\right]\right]}$$

$$\rightarrow\begin{cases}56\zeta(3)/\pi^4\approx 0.691, & \text{for } T\tau\ll 1,\\ 8\pi^2(\tau T)^2/[7\zeta(3)]\approx 9.384(\tau T)^2, & \text{for } T\tau\gg 1\ ,\end{cases}\tag{20}$$

is a function of τT only.

D. The Maki-Thompson contribution

We now consider the Maki-Thompson (MT) contribution (diagram 2 of Fig. 1) to the c-axis fluctuation conductivity. The contributions from the two other diagrams of the MT type (diagrams 3 and 4 of Fig. 1) are negligible, because they are of the same order in transmittance as is this diagram, but are less singular in ϵ. As was stated in Ref. 9, even when the pair lifetime τ_ϕ is short, this contribution is proportional to J^4 for small J above T_0, but is less singular above T_0 than the AL diagram, and was therefore excluded from that treatment. As we shall show in the following, the approximation of neglecting the MT diagram is usually justified. Nevertheless, there are a variety of possibilities relevant to the importance of the MT diagram, depending upon the material parameters. Depending upon τ_ϕ, the MT contribution to the transverse conductivity can have different temperature dependences, and its order in the interlayer transmittance can vary. For completeness, we consider the scattering lifetime τ and the pair-breaking lifetime τ_ϕ to be arbitrary, but satisfying $\tau_\phi>\tau$. We write

$$Q_{\alpha\beta}^{\mathrm{MT}}(\omega_\nu)=2e^2T\sum_{\omega_\mu}\int\frac{d^3q}{(2\pi)^3}L(q,\omega_\mu)I_{\alpha\beta}(q,\omega_\mu,\omega_\nu)\ ,\tag{21}$$

where

$$I_{\alpha\beta}(q,\omega_\mu,\omega_\nu)=T\sum_{\omega_n}\int\frac{d^3p}{(2\pi)^3}v_\alpha(p)v_\beta(q-p)C(q,\omega_{n+\nu},\omega_{\mu-n-\nu})C(q,\omega_n,\omega_{\mu-n})\\ \times G(p,\omega_{n+\nu})G(p,\omega_n)G(q-p,\omega_{\mu-n-\nu})G(q-p,\omega_{\mu-n})\ .\tag{22}$$

The MT contribution to the in-plane fluctuation conductivity $\sigma_{xx}^{\mathrm{MT}}$ was calculated in the dirty limit for a layered superconductor without pair breaking in Ref. 27,

$$\sigma_{xx}^{\mathrm{MT}}=\frac{e^2}{4s\epsilon}\ln\left[\frac{\epsilon^{1/2}+(\epsilon+r)^{1/2}}{r^{1/2}}\right]\ .\tag{23}$$

Equation (23) indicates that in the weak pair-breaking limit, the MT diagram makes an important contribution to the longitudinal fluctuation conductivity: it is of the same order as the AL contribution in the 3D regime, but is larger than the AL contribution in the 2D regime above T_0. For finite pair breaking, (23) is reduced in magnitude, however. As for the DOS contribution, in the vicinity of T_c, it is possible to take the static limit of the MT diagram simply by setting $\omega_\mu=0$ in (21). Although dynamic effects can be important for the longitudinal fluctuation conductivity well above T_0, the static limit is correct very close to T_c, as shown in Refs. 29 and 30.

We now consider the calculation of the MT contribution to the transverse conductivity. From the forms of $v_z(p)$ and $v_z(q-p)$ in (22) obtained from (5), the bare electromagnetic vertices are proportional to

$$\sin(p_zs)\sin(q_z-p_z)s\ .$$

After integration over the momentum $p=(\mathbf{p},p_z)$, the nonvanishing contribution is proportional to $\cos q_zs$. We take the limit $J\tau\ll 1$ in evaluating the remaining integrals, which may then be performed exactly.

In evaluating the sums over the remaining Matsubara frequencies ω_n in (22), it is useful to break up the sum into two parts. In the first part, ω_n is in the domains $]-\infty,-\omega_\nu[$ and $[0,\infty[$. This gives rise to the *regular* part of the MT diagram,

$$\begin{aligned}\sigma_{zz}^{\mathrm{MT(reg)}}&=-\frac{e^2s^2\pi r\tilde{\kappa}}{4}\int\frac{d^3q}{(2\pi)^3}\frac{\cos q_zs}{\epsilon+\eta\mathbf{q}^2+(r/2)(1-\cos q_zs)}\\ &=-\frac{e^2s\pi\tilde{\kappa}}{2}\int\frac{d^2\mathbf{q}}{(2\pi)^2}\left[\frac{\epsilon+\eta\mathbf{q}^2+r/2}{[(\epsilon+\eta\mathbf{q}^2)(\epsilon+\eta\mathbf{q}^2+r)]^{1/2}}-1\right]\\ &=-\frac{e^2sr\tilde{\kappa}}{16\eta}\left[\frac{(\epsilon+r)^{1/2}-\epsilon^{1/2}}{r^{1/2}}\right]^2\\ &\rightarrow-\frac{e^2sr\tilde{\kappa}}{16\eta}\begin{cases}1 & \text{for } \epsilon\ll r,\\ r/(4\epsilon) & \text{for } \epsilon\gg r\ ,\end{cases}\end{aligned}\tag{24}$$

where

$$\tilde{\kappa}=\frac{-\psi'\left[\frac{1}{2}+\frac{1}{4\pi T\tau}\right]+\psi'\left[\frac{1}{2}\right]+\frac{1}{4\pi T\tau}\psi''\left[\frac{1}{2}\right]}{\pi^2\left[\psi\left[\frac{1}{2}+\frac{1}{4\pi\tau T}\right]-\psi\left[\frac{1}{2}\right]-\frac{1}{4\pi\tau T}\psi'\left[\frac{1}{2}\right]\right]}$$

$$\rightarrow\begin{cases}28\zeta(3)/\pi^4\approx 0.3455 & \text{for } T\tau\ll 1,\\ \pi^2/[14\zeta(3)]\approx 0.5865 & \text{for } T\tau\gg 1\end{cases}\tag{25}$$

is another function only of τT. We note that this regular MT term is negative, as is the overall DOS contribution. However, it is smaller in magnitude than is the DOS contribution, and therefore makes a relatively small contribution to the overall fluctuation conductivity and to the temperature of the resistive maximum. In the 3D regime below T_0, it is proportional to J^2 and, in the 2D regime above T_0, it is proportional to J^4.

The second (*anomalous*) part of the MT diagram arises from the summation over ω_n in the domain $[-\omega_\nu, 0[$. In this domain, analytic continuation leads to an additional diffusive pole in the integration over q, with a characteristic pair-breaking lifetime τ_ϕ. This anomalous part of the MT diagram gives rise to

$$\begin{aligned}\sigma_{zz}^{\mathrm{MT(an)}}&=\frac{\pi e^2J^2s^2\tau}{4}\int\frac{d^3q}{(2\pi)^3}\frac{\cos q_zs}{(1/\tau_\phi+D\hat{Q}^2)[\epsilon+\eta\mathbf{q}^2+(r/2)(1-\cos q_zs)]}\\ &=\frac{\pi e^2s}{4(\epsilon-\gamma)}\int\frac{d^2\mathbf{q}}{(2\pi)^2}\left[\frac{\gamma+\eta\mathbf{q}^2+r/2}{[(\gamma+\eta\mathbf{q}^2)(\gamma+\eta\mathbf{q}^2+r)]^{1/2}}-\frac{\epsilon+\eta\mathbf{q}^2+r/2}{[(\epsilon+\eta\mathbf{q}^2)(\epsilon+\eta\mathbf{q}^2+r)]^{1/2}}\right]\\ &=\frac{e^2s}{16\eta}\left[\frac{\gamma+r+\epsilon}{[\epsilon(\epsilon+r)]^{1/2}+[\gamma(\gamma+r)]^{1/2}}-1\right],\end{aligned}\tag{26}$$

where

$$\gamma=\frac{2\eta}{v_F^2\tau\tau_\phi}\rightarrow\frac{\pi}{8T\tau_\phi}\begin{cases}1 & \text{for } T\tau\ll 1,\\ 7\zeta(3)/(2\pi^3T\tau) & \text{for } T\tau\gg 1\ .\end{cases}\tag{27}$$

In examining the limiting cases of (26), it is useful to consider the cases of weak ($\gamma\ll r$ or $J^2\tau\tau_\phi\gg\frac{1}{2}$) and strong ($\gamma\gg r$ or $J^2\tau\tau_\phi\ll\frac{1}{2}$) pair breaking separately. For weak pair-breaking, we have

$$\sigma_{zz}^{\mathrm{MT(an)}}\rightarrow\frac{e^2s}{16\eta}\begin{cases}(r/\gamma)^{1/2} & \text{for } \epsilon\ll\gamma\ll r,\\ (r/\epsilon)^{1/2} & \text{for } \gamma\ll\epsilon\ll r,\\ r/(2\epsilon) & \text{if } \gamma\ll r\ll\epsilon\ .\end{cases}\tag{28}$$

In this case, there is the usual 3D to 2D dimensional crossover in the anomalous MT contribution at T_0, for which $\epsilon(T_0)=r$. There is an additional crossover at T_1 (where $T_c<T_1<T_0$), characterized by $\epsilon(T_1)=\gamma$, below which the anomalous MT term saturates. Below T_0, the MT contribution is proportional to J, but in the 2D regime above T_0 it is proportional to J^2.

For strong pair breaking,

$$\sigma_{zz}^{\mathrm{MT(an)}}\rightarrow\frac{e^2s}{32\eta}\begin{cases}r/\gamma & \text{for } \epsilon\ll r\ll\gamma,\\ r^2/(4\gamma\epsilon) & \text{for } r\ll\min(\epsilon,\gamma)\ .\end{cases}\tag{29}$$

In this case, the 3D regime (below T_0) is not singular, and the anomalous MT contribution is proportional to J^2, rather than J for weak pair breaking. In the 2D regime, it is proportional to J^4 for strong pair breaking, as opposed to J^2 for weak pair breaking. In addition, the overall magnitude of the anomalous MT contribution with strong pair breaking is greatly reduced from that for weak pair breaking.

Let us now compare the regular and anomalous MT contributions. Since these contributions are opposite in sign, it is important to determine which will dominate. Since we expect $\tau_\phi\gg\tau$, strong pair breaking is most likely applicable to the dirty limit. When the pair breaking is weak, the anomalous term is always of lower order in J than is the regular term, so the regular term can be neglected. This is true for both the clean and dirty limits. The most important regime for the regular MT term is the dirty limit with strong pair breaking. In this case, when $\tau_\phi T\sim 1$, the regular and anomalous terms are comparable in magnitude. In short, it is usually a good approximation to neglect the regular term, except in the dirty limit with relatively strong pair breaking. However, we include it for generality.

As discussed in greater detail in Sec. V, when $J\tau\ll 1$, the effective interlayer tunneling rate is on the order of $J^2\tau$. When $1/\tau_\phi\ll J^2\tau\ll 1/\tau$, the quasiparticles scatter many times before tunneling to the neighboring layers,[21] and the pairs live long enough for them to tunnel coherently. When $J^2\tau\ll 1/\tau_\phi$, the pairs decay before both paired quasiparticles tunnel.

It is interesting to compare the anomalous MT contribution with the DOS and AL contributions. This comparison is best made in the 2D regime above T_0. For weak pair breaking, the anomalous MT and DOS terms are proportional to J^2, but opposite in sign, and the former has a stronger temperature dependence than the latter. With strong pair breaking, the anomalous MT and AL contributions are proportional to J^4, but the former is less singular in $\epsilon\ll 1$ than is the latter. Hence, the MT contribution is in some sense *intermediate* between the DOS and AL contributions. Nevertheless, as shown in the following, the MT contribution can be important in the overall temperature dependence of the resistivity, eliminating the peak for weak pair breaking.

E. Full transverse fluctuation conductivity

From the previous sections, the full zero-field transverse fluctuation conductivity is found to be

$$\sigma_{zz}^{\mathrm{fl}}=\sigma_{zz}^{\mathrm{AL}}+\sigma_{zz}^{\mathrm{DOS}}+\sigma_{zz}^{\mathrm{MT(reg)}}+\sigma_{zz}^{\mathrm{MT(an)}}$$
$$=\frac{e^2 s}{16\eta}\left[-r\kappa\ln\left[\frac{2}{\epsilon^{1/2}+(\epsilon+r)^{1/2}}\right]^2+[(\epsilon+r)^{1/2}-\epsilon^{1/2}]^2\left[\frac{1}{4[\epsilon(\epsilon+r)]^{1/2}}-\tilde{\kappa}\right]\right.$$
$$\left.+\left[\frac{\epsilon+\gamma+r}{[\epsilon(\epsilon+r)]^{1/2}+[\gamma(\gamma+r)]^{1/2}}-1\right]\right]. \tag{30}$$

We note that the second term in (30) contains both the AL and the regular MT contributions. Writing the AL term in this fashion, it is easy to see that the AL term is generally larger in magnitude than is the regular MT term, except for $r \ll \epsilon \approx 1$.

Since there is a competition between the negative (DOS and regular MT) and positive (AL and anomalous MT) terms, there can be a maximum in the fluctuation resistivity (minimum in the fluctuation conductivity). Since the temperature dependences of r, κ, and $\tilde{\kappa}$ are weak compared with that present in ϵ, to obtain the position of the maximum, it suffices to optimize (30) with respect to ϵ. Using the restriction $J\tau \ll 1$ for the validity of our theory, it suffices to consider the cases in which the resistive maximum occurs in the 2D regime. Setting $\epsilon=\epsilon_m$ at $T=T_m$, we have

$$\frac{\epsilon_m}{r}\approx\frac{1}{(8r\kappa)^{1/2}}-\frac{1}{8\kappa}\left[\tilde{\kappa}-\frac{1}{2\gamma}\right], \tag{31}$$

which is satisfied for $r\kappa \ll 1$ and $\gamma\kappa > 1$.

As can be seen from the above analysis, the regular MT term decreases the position of the maximum somewhat, but the anomalous term increases it somewhat. It is then qualitatively correct to neglect the MT terms altogether, but quantitatively, they can change the overall shape of the fluctuation resistivity. We remark that there may be cases in which T_m could occur in the 3D regime, but such cases cannot be addressed by our theory, as they would require a proper treatment of nonlocal effects, as well as the removal of the restriction $J\tau \ll 1$.

In Figs. 2 and 3, we have plotted ρ_{zz}/ρ_{zz}^N versus T/T_{c0} for various values of the scattering lifetime τT_{c0} and the pair-breaking lifetime $\tau_\phi T_{c0}$. In these figures, we have taken $\rho_{zz}^N=\frac{1}{2}N(0)J^2e^2s^2\tau$, as described at the end of Sec. II B. In these and subsequent figures, the solid curves are plots of ρ_{zz}/ρ_{zz}^N. For comparison, the dashed curves are plots of ρ_{xx}/ρ_{xx}^N, for the same sets of parameters. The formulas relevant for the in-plane conductivities (and hence ρ_{xx}) are given in Sec. IV. In Fig. 2, we have chosen $\tau T_{c0}=1$, which is relevant for the high-T_c cuprates. In each of these figures, curves for $\tau_\phi T_{c0}=1$, 10, and 100 are shown. We have chosen $r(T_{c0})=0.1$, 0.01, and 0.001 in Figs. 2(a), 2(b), and 2(c), respectively. These values correspond roughly to those expected for YBCO, BSCCO, and $\mathrm{Tl_2Ba_2CaCu_2O_{8+\delta}}$ (TBCCO), respectively. In order that the overall fluctuation conductivity not give a large correction to the normal-state conductivity at temperatures well above the transition (i.e., for $T > 1.03T_{c0}$), we have chosen $E_F/T_{c0}=300$ for $r(T_{c0})=0.1$ and 0.01 [Figs. 2(a) and 2(b)], but $E_F/T_{c0}=500$ for $r(T_{c0})=0.001$ [Fig. 2(c)]. As can be seen from each of these figures, for a fixed amount of pair breaking and intralayer scattering, strong pair breaking (e.g., $\tau_\phi T_{c0}=1$) gives rise to a peak, or maximum in ρ_{zz}/ρ_{zz}^N. A small, broad peak in ρ_{xx}/ρ_{xx}^N can also occur, but only for weak anisotropy $[r(T_{c0})=0.1]$ and for such strong pair breaking $(\tau_\phi T_{c0}=1)$. Increasing the anisotropy [or decreasing $r(T_{c0})$] greatly enhances the magnitude of the peak in ρ_{zz}/ρ_{zz}^N. Decreasing the amount of pair breaking decreases the amplitude of the peak, as seen in each figure.

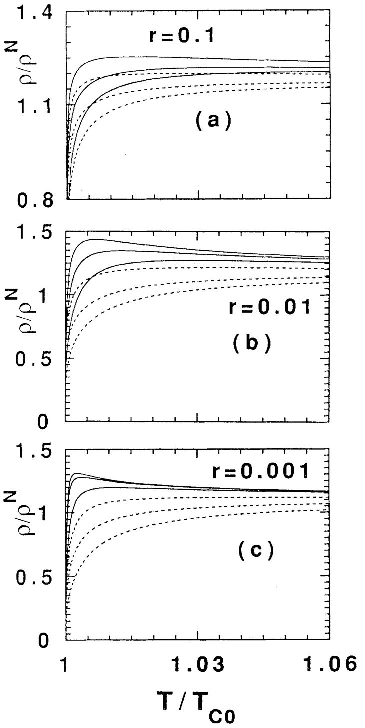

FIG. 2. Shown are plots of the zero-field normalized resistivities ρ_{xx}/ρ_{xx}^N (dashed curves) and ρ_{zz}/ρ_{zz}^N (solid curves) versus T/T_{c0} for $\tau T_{c0}=1$ and for $\tau_\phi T_{c0}=1$ (top curves), $\tau_\phi T_{c0}=10$ (middle curves), and $\tau_\phi T_{c0}=100$ (bottom curves). In all plots, temperatures shown are for $1 \le T/T_{c0} \le 1.06$. (a) $r(T_{c0})=0.1$, $E_F/T_{c0}=300$. (b) $r(T_{c0})=0.01$, $E_F/T_{c0}=300$. (c) $r(T_{c0})=0.001$, $E_F/T_{c0}=500$.

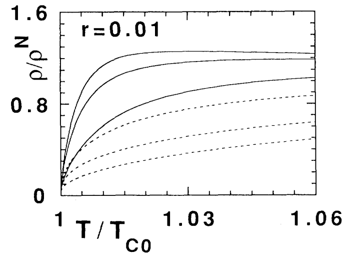

FIG. 3. Plots of the zero-field ρ_{zz}/ρ_{zz}^N (solid curves) and ρ_{xx}/ρ_{xx}^N (dashed curves) vs T/T_{c0} for $r(T_{c0})=0.01$, $E_F/T_{c0}=300$, $\tau T_{c0}=0.1$, and $\tau_\phi T_{c0}=1$, 10, and 100, in order from top to bottom.

In Fig. 3, plots with the same parameters as in Fig. 2(b) are shown, except that the intralayer scattering lifetime has been decreased to $\tau T_{c0}=0.1$, which is in the dirty limit. Hence, it can be seen that the magnitude of the peak in ρ_{zz}/ρ_{zz}^N is reduced by interlayer hopping, by intralayer scattering, and by pair breaking. For highly anisotropic materials, no peak in ρ_{xx}/ρ_{xx}^N is expected for any amount of pair breaking shown in these figures.

We remark that these zero-field results are at least qualitatively consistent with experiments on cuprate superconductors. In YBCO, the best samples showed no peak[4] (or at best, a very small peak[5]) in ρ_{zz}, which is consistent with our $\tau T_{c0}=1$, $\tau_\phi T_{c0}=10$ curve with $r(T_{c0})=0.1$ [Fig. 2(a)]. In BSCCO, the substantial peak observed in Ref. 7 is consistent with our $\tau T_{c0}=1$ and $\tau_\phi T_{c0}=1,10$ curves for $r(T_{c0})=0.01$ [Fig. 2(b)]. To elucidate which of these curves give a better representation of the data, it is useful to examine the magnetic field dependence, which will be done in the following.

F. Higher-order corrections

For completeness, we have considered the possible role of diagram 11 of Fig. 1. This term can become important in extremely anisotropic layered superconductors, especially in high-T_c materials if the mechanism proves to be electronic in origin. Specifically, diagram 11 is important for

$$J^2\tau/T_{c0} \ll 1/(E_F\tau)^{2/3}$$

in the dirty limit,[17] which can occur if $r(T_{c0})$ is extremely small. In this paper, we have neglected such diagrams, and have chosen compensatingly rather large values of $E_F\tau$.

III. MAGNETIC-FIELD EFFECTS

We now consider the effect of a magnetic field parallel to the c axis, or normal to the layers. For a more general field direction, the situation is considerably more complicated, and will be discussed elsewhere.[26] For this particular field direction, however, the vertices do not depend upon the magnetic field, and both the quasiparticles and the pairs form Landau orbits within the layers. The c-axis dispersion remains unchanged from the zero-field form. Such a configuration was discussed previously.[3,21]

For this simple field direction, it is elementary to generalize our zero-field results to finite field strengths.[3,21,32] In the integral expressions for the various diagrammatic contributions, one replaces

$$\eta \mathbf{q}^2 \rightarrow \eta(\nabla/i - 2e\,\mathbf{A})^2 \tag{32}$$

in each of the integral expressions for the contributions to the fluctuation conductivity. With $\mathbf{B}=B\hat{\mathbf{z}}$, we may choose $\mathbf{A}=\frac{1}{2}B(-y,x,0)$, and hence $\eta\mathbf{q}^2$ becomes the Hamiltonian of the simple harmonic oscillator. The pair wave functions $|\phi_n(\mathbf{r})\rangle$ are the usual harmonic-oscillator eigenfunctions, satisfying

$$f[\eta(\nabla/i-2e\,\mathbf{A})^2]|\phi_n(\mathbf{r})\rangle = f(E_n)|\phi_n(\mathbf{r})\rangle\ , \tag{33}$$

where

$$E_n=\beta(n+1/2) \tag{34}$$

and

$$\beta = 4\eta e B = \frac{2B\eta}{T_c\eta|_{T_c}|dH_{c2,\perp}(T)/dT|_{T_c}}\ , \tag{35}$$

and

$$T_c|dH_{c2,\perp}(T)/dT|_{T_c} = \Phi_0/[2\pi\xi_\parallel^2(0)]$$

is the extrapolation of the upper critical field perpendicular to the layers to zero temperature from its slope near T_c, written in terms of the flux quantum Φ_0 and the zero-temperature Ginzburg-Landau coherence length parallel to the layers $\xi_\parallel(0)$. The two-dimensional integration over $\mathbf{q}$ is replaced by a summation over the Landau levels (indexed by n), taking account of the Landau degeneracy factor in the usual way [32],

$$\int \frac{d^2\mathbf{q}}{(2\pi)^2} \rightarrow \frac{T}{\Phi_0}\sum_n = \frac{\beta}{4\pi\eta}\sum_n\ , \tag{36}$$

where $n=0,1,2,\ldots$. The 1/2 in (34) can be incorporated into ϵ, by measuring temperature with respect to the mean-field $T_c(B)$. This results in

$$\epsilon_B = \epsilon + \beta/2 \approx \ln[T/T_c(B)]\ .$$

For completeness, we write the full expressions in the presence of an arbitrary field in the c-axis direction. We have

$$\sigma_{zz}^{\rm AL} = \frac{e^2 s r^2 \beta}{128\eta}\sum_{n=0}^{\infty}\frac{1}{[(\epsilon_B+\beta n)(\epsilon_B+\beta n+r)]^{3/2}}\ , \tag{37}$$

$$\sigma_{zz}^{\rm DOS} = -\frac{e^2 s r \kappa \beta}{16\eta}\sum_{n=0}^{1/\beta}\frac{1}{[(\epsilon_B+\beta n)(\epsilon_B+\beta n+r)]^{1/2}}\ , \tag{38}$$

$$\sigma_{zz}^{\rm MT(reg)} = -\frac{e^2 s \tilde{\kappa} \beta}{8\eta}\sum_{n=0}^{\infty}\left[\frac{\epsilon_B+\beta n+r/2}{[(\epsilon_B+\beta n)(\epsilon_B+\beta n+r)]^{1/2}}-1\right]\ , \tag{39}$$

and

$$\sigma_{zz}^{\mathrm{MT(an)}}=\frac{e^2 s\beta}{16\eta(\epsilon-\gamma)}\sum_{n=0}^{\infty}\left[\frac{\gamma_B+\beta n+r/2}{[(\gamma_B+\beta n)(\gamma_B+\beta n+r)]^{1/2}}-\frac{\epsilon_B+\beta n+r/2}{[(\epsilon_B+\beta n)(\epsilon_B+\beta n+r)]^{1/2}}\right], \tag{40}$$

where $\gamma_B=\gamma+\beta/2$ is defined analogously to ϵ_B for simplicity of expression. We note that (37) was obtained previously.[3] In numerical evaluation of (40), it is useful to manipulate the expression algebraically, in order to remove the apparent (but spurious) singularity when $\epsilon-\gamma\approx 0$. In order that the DOS term have a smooth temperature dependence at fixed field strength, we have used a Gaussian cutoff instead of a sharp cutoff in our numerical evaluations of (38). Expansions of (37)–(40) for weak and strong fields are given in the Appendix.

IV. FLUCTUATION CONDUCTIVITY PARALLEL TO THE LAYERS

In Sec. III, we showed that the resistivity transverse to the layers can exhibit a peak above $T_c(B)$, which peak is enhanced in magnitude (as well as shifted to lower temperatures) in a magnetic field. Since the experiments which show this effect for the transverse resistivity do not show the same effect for the parallel resistivity, the question arises as to whether the density of states diagram might also lead to such a peak in the parallel resistivity. In order to check this point, we have evaluated the same diagrams as above for the parallel fluctuation conductivity in a field perpendicular to the layers. Since all but the density of states diagram (which is simply proportional to that calculated above) have been evaluated previously, we shall simply list the results. We have

$$\sigma_{xx}^{\mathrm{AL}}=\frac{e^2}{4s}\sum_{n=0}^{\infty}(n+1)\left[\frac{1}{[(\epsilon_B+\beta n)(\epsilon_B+\beta n+r)]^{1/2}}-\frac{2}{\{[\epsilon_B+\beta(n+\frac{1}{2})][\epsilon_B+\beta(n+\frac{1}{2})+r]\}^{1/2}}+\frac{1}{\{[\epsilon_B+\beta(n+1)][\epsilon_B+\beta(n+1)+r]\}^{1/2}}\right], \tag{41}$$

$$\sigma_{xx}^{\mathrm{DOS}}+\sigma_{xx}^{\mathrm{MT(reg)}}=-\frac{e^2\beta(\kappa+\tilde{\kappa})}{4s}\sum_{n=0}^{1/\beta}\frac{1}{[(\epsilon_B+\beta n)(\epsilon_B+\beta n+r)]^{1/2}}, \tag{42}$$

and

$$\sigma_{xx}^{\mathrm{MT(an)}}=\frac{e^2\beta}{8s(\epsilon-\gamma)}\sum_{n=0}^{\infty}\left[\frac{1}{[(\gamma_B+\beta n)(\gamma_B+\beta n+r)]^{1/2}}-\frac{1}{[(\epsilon_B+\beta_n)(\epsilon_B+\beta n+r)]^{1/2}}\right]. \tag{43}$$

Note that we have included the DOS and regular MT terms together, as they are proportional to each other for this conductivity tensor element, and the DOS diagram differs from that for the transverse conductivity by the factor $(v_F/sJ)^2$, which measures the square of the ratio of the effective Fermi velocities. The same factor enters into the normal-state conductivity, leading to the standard

$$\sigma_{xx}^{N}=\tfrac{1}{2}N(0)e^2v_F^2\tau=E_F\tau e^2/(2\pi s)\ .$$

We note that (41) was given previously in Ref. 3, using standard procedures,[32] and rederived in Ref. 33, and (43) was also given previously.[33,34] As in (38), we have used a Gaussian cutoff in (42) in our numerical evaluations, in order to insure a smooth temperature dependence of the parallel conductivity at fixed field strength. In addition, it is useful to manipulate (43) algebraically, in order to remove the apparent (but spurious) singularity at $\epsilon=\gamma$, as was done in (40), leading to the zero-field result (26). The low-field expansions of (41)–(43) are given in the Appendix.

We note that the new (DOS) correction we have included gives rise to the term proportional to κ in (42). In the dirty limit, since $\kappa\rightarrow 0.691$ and $\tilde{\kappa}\rightarrow 0.3455$, the DOS contribution is not much larger than the (relatively small) regular MT term, and was therefore neglected by all previous workers. However, when $\tau T_{c0}=1$, $\kappa(T_{c0})=14.3123$, which is much larger than $\tilde{\kappa}(T_{c0})=0.5578$, so the DOS contribution *cannot* be neglected relative to the other terms. Hence, fits to data in which the DOS term has been neglected can only be trusted for systems which are in the dirty limit. Since the cuprates are thought to have $\tau T_{c0}\approx 1$, it is necessary to include the DOS contribution in the fits. This term dramatically alters the shape of the overall parallel resistivity, even for zero magnetic field. This change in ρ_{xx} due to the inclusion of the DOS contribution is pictured in Fig. 4. In this figure, we have plotted ρ_{xx}/ρ_{xx}^{N} for $\tau T_{c0}=1$, $\tau_\phi T_{c0}=10$, and $E_F/T_{c0}=300$, for both $r(T_{c0})=0.1$ (dashed curves), and $r(T_{c0})=0.01$ (solid curves), both with and without the DOS contribution. As is easily seen from Fig. 4, the DOS contribution greatly alters the overall resistivity, with the main aspect of the alteration being an overall increase in the resistivity. However, as can be seen by comparing all four curves, there is an additional nontrivial temperature dependence

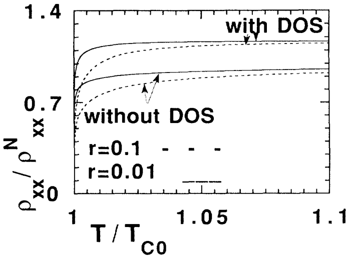

FIG. 4. Plots of ρ_{xx}/ρ_{xx}^N vs T/T_{c0} in zero magnetic field, for $E_F/T_{c0}=300$, $\tau T_{c0}=1$, $\tau_\phi T_{c0}=10$, and for $r(T_{c0})=0.1$ (dashed curves) and 0.01 (solid curves), with (top curves) and without (bottom curves) the density of states contribution.

which enters into the fluctuation resistivity, which is significant enough to alter all fits to experimental data. Since to date no fits to any data for ρ_{xx} have included the DOS contribution, all such fits could require substantial revision.

V. DISCUSSION

In comparison of our theory with experiment, it is important to keep in mind that we have included the leading contributions to the conductivity arising from fluctuations of the order parameter about its mean-field value [which vanishes at $T_c(B)$], but have not included the critical fluctuations of the order parameter, which cause the order parameter to be nonvanishing at the mean-field $T_c(B)$. In treatments of the critical fluctuations such as the self-consistent Hartree approximation[12] and more complete treatments,[11] the main effect is a shift of the mean-field $T_c(B)$ to zero, with a corresponding broadening of the transition. This broadening of the transition increases strongly with increasing magnetic field strength, in qualitative agreement with experiments on the cuprates. Hence, in examining the calculations we have performed, one should mentally broaden the transitions, the amount of broadening increasing strongly with the field strength.

While it is difficult to know precisely what values of E_F/T_{c0} to choose, one would like to be able to choose values consistent either with band structure calculations or with photoemission experiments. Unfortunately, we are limited by the restriction that the fluctuation conductivity makes a small correction to the overall conductivity. Since we have neglected higher-order density of states corrections (such as diagram 11 of Fig. 1), we are thus forced to choose values for E_F/T_{c0} corresponding to $E_F\sim 1-5$ eV, larger than expected from such extractions. Choosing E_F/T_{c0} in closer agreement with band-structure calculations or photoemission experiments would greatly enhance the DOS corrections from those exhibited in our calculations.

We note that the pair-breaking parameter $\tau_\phi T_{c0}$ which enters the anomalous MT contributions also affects the zero-field transition temperature, which is then obtained from the vanishing of the inverse propagator (6) by replacing $|\omega_\mu|$ with $1/\tau_\phi$ and setting $\alpha_q=0$ at $T=T_{c0}$. For moderate pair-breaking strengths ($\tau_\varphi T_{c0}\sim 10$), such corrections can be incorporated with reasonable accuracy by redefining T_{c0} to be the actual zero-field transition temperature, rather than the zero-field transition temperature in the absence of pair breaking. For strong pair breaking ($\tau_\phi T_{c0}\sim 1$), inclusion of the pair-breaking parameter in the fluctuation propagator (6) with $\alpha_q\neq 0$ enhances the effect of the magnetic field present in α_q. We have neglected such enhancement effects in our numerical calculations, treating T_{c0} as the effective zero-field transition temperature.

In Figs. 5–7, we have plotted ρ_{zz}/ρ_{zz}^N and ρ_{xx}/ρ_{xx}^N versus T/T_{c0} in zero field and at fields corresponding to $\beta(T_{c0})=0.05$ and 0.10. In these figures, we have chosen $r(T_{c0})=0.01$ and $E_F/T_{c0}=300$, which corresponds roughly to the cuprate BSCCO. Similar calculations have been carried out (but are not pictured) for $r(T_{c0})=0.1$ and $E_F/T_{c0}=300$, and for $r(T_{c0})=0.001$ with $E_F/T_{c0}=500$, which correspond roughly to YBCO and TBCCO, respectively. In Fig. 5, the additional parameters are $\tau T_{c0}=\tau_\phi T_{c0}=1$, which is appropriate for the case of strong pair breaking. We note that the peak in ρ_{zz}/ρ_{zz}^N increases dramatically with increasing field, but the curves do not coincide with each other above the peaks, in contrast to the experiments.[7] Even with the expected field broadening due to critical fluctuations, it is difficult to imagine how the behavior of ρ_{xx}/ρ_{xx}^N in Fig. 5 could be consistent with experiments on BSCCO. In addition, the falloff in ρ_{xx}/ρ_{xx}^N just below the peak in the $\beta(T_{c0})=0.10$ curve is very sharp, unlike the experiments. Similar but more pronounced behavior for ρ_{zz}/ρ_{zz}^N is found for $r(T_{c0})=0.001$, but for $r(T_{c0})=0.1$, the increase in the peak in ρ_{zz}/ρ_{zz}^N with increasing field is almost negligible. For both $r(T_{c0})=0.1$ and 0.001, ρ_{xx}/ρ_{xx}^N at $\beta(T_{c0})=0.10$ has a sharp falloff, as in Fig. 5. Hence, we argue that such strong pair breaking (as has been suggested previously,[24,25] is inconsistent with the strong-field experiments on both YBCO and BSCCO.

Note that in previous fits,[24,25] the authors used the low-field expansion and neglected the DOS contribution, but included the very small Zeeman (or Pauli) corrections, which we have omitted. We used the full perpendicular field expressions (37)–(43), which are accurate for larger field strengths. Another difference in the theories is that nonlocal corrections were included in Ref. 24, which corrections we have neglected. In addition, fits in

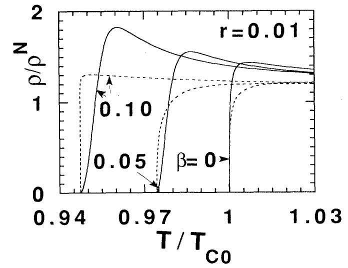

FIG. 5. Plots of the normalized resistivities ρ_{zz}/ρ_{zz}^N (solid curves) and ρ_{xx}/ρ_{xx}^N (dashed curves) vs T/T_{c0}, for $r(T_{c0})=0.01$, $E_F/T_{c0}=300$, and $\tau T_{c0}=\tau_\phi T_{c0}=1$, at field values corresponding to $\beta(T_{c0})=0$, 0.05, and 0.10.

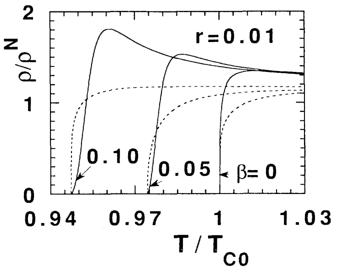

FIG. 6. Plots of ρ_{zz}/ρ_{zz}^N (solid curves) and ρ_{xx}/ρ_{xx}^N (dashed curves) vs T/T_{c0}, for $r(T_{c0})=0.01$, $E_F/T_{c0}=300$, $\tau T_{c0}=1$, and $\tau_\phi T_{c0}=10$, at field values corresponding to $\beta(T_{c0})=0$, 0.05, and 0.10.

Refs. 24 and 25 included the case of the field parallel to the layers. However, in those fits the orbital magnetic-field pair breaking (the *dominant* term for weak fields[26] such as in the experiments[7]) was omitted, so the extracted pair-breaking strength was assumed to originate from the Zeeman energy splitting. However, we argue that for $\beta(T_{c0})=0.10$, we are still in the regime $H \ll H_P \sim 150$ T where such Zeeman corrections are negligible, regardless of the field direction.[21,26]

In Fig. 6, we have plotted ρ_{zz}/ρ_{zz}^N and ρ_{xx}/ρ_{xx}^N for the same parameters as in Fig. 5, except that $\tau_\phi T_{c0}=10$, which corresponds to intermediate strength pair breaking. We note that the ρ_{zz}/ρ_{zz}^N curves do not fall exactly on top of one another, but come closer to one another than in the strong pair-breaking case (Fig. 5). In addition, the ρ_{xx}/ρ_{xx}^N curve for $\beta(T_{c0})=0.10$ is much more rounded than in Fig. 5, further suggesting that intermediate-strength pair breaking is more consistent with the experiments on BSCCO than is weak pair breaking. While we are not aware of similar experiments on TBCCO, assuming $r(T_{c0})\approx 0.001$ and the same values for τT_{c0} and $\tau_\phi T_{c0}$, our calculations (not pictured) suggest that the peak in ρ_{zz}/ρ_{zz}^N will be much stronger than in BSCCO, but that the curves will probably not lie on top of one another above the peak temperatures. In addition, our calculation for $r(T_{c0})=0.1$ (not pictured) also shows more rounded ρ_{xx}/ρ_{xx}^N at $B(T_{c0})=0.10$, more consistent with experiments on YBCO than the strong pair-breaking calculations.

In Fig. 7, we have made similar plots for the dirty limit case $\tau T_{c0}=0.1$, with moderate pair-breaking, $\tau_\phi T_{c0}=10$. In this case the importance of the DOS contribution is considerably reduced. In all such curves we have obtained, there is no peak in ρ_{xx}/ρ_{xx}^N, and both ρ_{zz}/ρ_{zz}^N and ρ_{xx}/ρ_{xx}^N curves broaden similarly in a field. Note that for such strong scattering, ρ_{xx}/ρ_{xx}^N exhibits a great deal of fluctuations above T_{c0}. In addition, the peak in ρ_{zz}/ρ_{zz}^N is much weaker than for $\tau T_{c0}=1$, being absent for $r(T_{c0})=0.1$ (not pictured). Furthermore, for $r(T_{c0})=0.01$ (Fig. 7) and 0.001 (not pictured), the ρ_{zz}/ρ_{zz}^N curves for different field values nearly fall on top of one another.

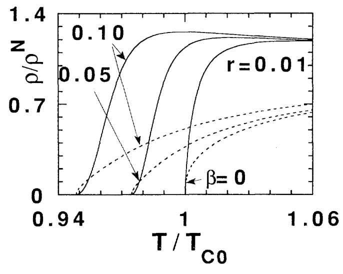

FIG. 7. Plots of ρ_{zz}/ρ_{zz}^N (solid curves) and ρ_{xx}/ρ_{xx}^N (dashed curves) vs T/T_{c0}, for $r(T_{c0})=0.01$, $E_F/T_{c0}=300$, $\tau T_{c0}=0.1$, and $\tau_\phi T_{c0}=10$, at field values corresponding to $\beta(T_{c0})=0$, 0.05, and 0.10.

While the field broadening of ρ_{xx}/ρ_{xx}^N in the dirty limit (Fig. 7) appears very similar to that observed in experiment (taking into account the further broadening due to critical fluctuations), one should not take these figures too seriously in regard to the cuprates, for which normal-state measurements are more consistent with relatively clean values $\tau T_{c0}\sim 1$, such as for Figs. 5 and 6. Hence, our calculations show that for $\tau T_{c0}=1$, the best agreement with experiments on YBCO and BSCCO is for *moderate* pair breaking ($\tau_\phi T_{c0}\sim 10$), rather than strong pair breaking ($\tau_\phi T_{c0}\sim 1$).

In this work, the model described by (1) assumes coherent quasiparticle interlayer propagation, which is reasonable in materials such as fully oxygenated YBCO, but could be questionable in highly anisotropic materials such as BSCCO. However, incoherent quasiparticle processes at randomly located positions $\mathbf{r}_{ij}$ can be included by adding a term to the single quasiparticle Hamiltonian of the form

$$\sum_{ij} \delta J_j(\mathbf{r}_i)\psi_j(\mathbf{r}_i)\psi_{j+1}^\dagger(\mathbf{r}_i) \ ,$$

plus its Hermitian conjugate, where $\delta J_j(\mathbf{r}_i)$ is the random part of the interlayer tunneling energy arising from microscopic electrical shorts, and $\psi_j(\mathbf{r}_i)$ is a Nambu spinor that annihilates a quasiparticle at the random position $\mathbf{r}_i$ between the jth and $(j+1)$th layers. Such processes complicate the situation considerably, but to leading order in $\langle(\delta J)^2\rangle$, where $\langle \cdots \rangle$ is an average over the random tunneling positions, lead to the replacement of J^2 by $J^2+\langle(\delta J)^2\rangle$.[36,37] Those authors were able to derive the effective Lawrence-Doniach free energy, but did not evaluate the fluctuation propagator, which involves multiple hopping (or interlayer scattering processes). In Ref. 37, the normal-state conductivity parallel to the layers was found to have a Drude-like frequency dependence, but $\sigma_{zz}(\omega)$ was found for $J=0$ to be independent of frequency, to lowest order in the random interlayer scattering. Otherwise, interlayer scattering and interlayer coherent tunneling gave nearly identical results for layered (periodic) superconductors. Hence, it is likely that the question of coherent versus incoherent tunneling is primarily a semantic one, as it may be difficult to distinguish these microscopic models, without accurate determination of the frequency dependence of the normal-state conductivity tensor, and accurate evaluation of the fluctuation propagator in the random short (or interlayer tunneling) model.

A recent treatment[38] of a single superconductor-insulator-superconductor junction is related to the coherent tunneling model. That treatment[38] was similar to that of Ref. 9, but involved the exact transmittance from one superconductor to the other, through the insulating barrier. They[38] also obtained a peak in ρ_{zz} at temperatures above T_c, in substantial agreement with our zero-field results obtained assuming coherent tunneling of periodic structures, using the perturbative approach in the fluctuation propagator. Thus, it appears that our perturbative approach gives the correction physics of the layered systems. However, we have not included higher-order diagrams, such as diagram 11 in Fig. 1. When the leading DOS contributions (diagrams 5–8) are comparable in magnitude to the normal-state conductivity, one must include all such higher-order processes,[17] which will modify the quantitative details of our results, but probably not the qualitative physics arising from our perturbative approach.

In this treatment, the normal state resistivities ρ_{xx}^N and ρ_{zz}^N are both assumed to have diffusive character, with effective diffusion constants $D_\parallel = v_F^2\tau/2$ parallel to the layers and $D_\perp = J^2 s^2 \tau/2$ normal to the layers. Ordinarily, if one expands $\hat{D}Q^2$ in (4) for small $q_z s \ll 1$, the propagation normal to the layers would be anisotropic, but diffusive in that direction as well as within the layers. However, for larger values of $q_z s \sim 1$, the c-axis propagation is not diffusive, due to the hopping character of the c-axis quasiparticle transport for lengths on the order of s. One might then wonder why $D_\perp$ turned out to be proportional to the intralayer scattering lifetime. This dependence can be understood by the following uncertainty argument.[39] Intralayer scattering with diffusion constant $D_\parallel$ leads to a smearing of the intralayer momentum

$$|\Delta \mathbf{p}| \sim 1/(D_\parallel \Delta t)^{1/2}$$

within the time interval Δt. Such an uncertainty in the intralayer momentum then leads to an uncertainty in the quasiparticle energy ΔE on the order of

$$v_F |\Delta \mathbf{p}| \sim 1/(\tau \Delta t)^{1/2} \ .$$

When $\Delta E > J$, or for times Δt such that $\Delta t \sim 1/(J^2\tau)$, hopping to the next layer a distance s away is possible. Writing $s \sim (D_\parallel \Delta t)^{1/2}$, we then have $D_\perp \sim J^2 s^2 \tau$, as in our model.

We have not taken into account the effects of weak localization arising either from predominantely two-dimensional propagation in the presence of disorder, or from disorder in the c-axis propagation. Two-dimensional localization can be included, but will be discussed elsewhere.[40] Such corrections are likely to be important in highly oxygen-deficient cuprates, for which the upturn in the c-axis resistivity occurs over a wide temperature range.

In conclusion, we have shown that the upturn in the c-axis resistivity just above T_c in highly anisotropic layered superconductors does not necessarily imply incoherent tunneling between the layers, as has been widely advertised.[41] Such behavior and its strong enhancement in a magnetic field normal to the layers are natural consequences of layered superconductors, even when the c-axis propagation is by coherent tunneling. Specifically, it arises from the decrease in the normal quasiparticle density of states due to fluctuations. In addition, our numerical calculations suggest that the pair-breaking rates in the cuprate superconductors are considerably less than those obtained previously.[24,25] This conclusion is significant, suggesting that the cuprate superconductors are not likely to be gapless at low temperatures (as suggested recently from transmission experiments[42]), at least from conventional pair-breaking mechanisms.

ACKNOWLEDGMENTS

The authors would like to thank A. A. Abrikosov, B. Al'tshuler, K. Gray, L. Ioffe, K. Levin, A. Rojo, A. Tartakovsky, and B. Veal for helpful discussions. This work was supported by the U.S. Department of Energy under Contract No. W-31-109-ENG-38.

APPENDIX

There are two regions of relevant field strengths,[32] the "weak"-field regime ($\beta \ll \epsilon_B$) and the "strong"-field regime ($\epsilon_B \ll \beta \ll 1$). In this appendix, we list analytic expressions for the contributions to the fluctuation conductivity in these field regimes. In the weak-field regime, we expand the various conductivity contributions in powers of B. Such expansions are facilitated by use of the Euler-Maclaurin approximation formula,

$$\sum_{n=0}^{N} f(n) = \int_0^N f(x)dx + \frac{1}{2}[f(N)+f(0)] + \tfrac{1}{12}[f'(N)-f'(0)] + \cdots \ . \tag{A1}$$

If one writes the expressions in terms of ϵ_B, then terms linear in B will appear. However, writing the expressions in terms of the zero field ϵ, all terms linear in B vanish identically, leaving the leading terms of order B^2. To order B^2, we find

$$\sigma_{zz}^{\mathrm{AL}} = \frac{e^2 s}{32\eta}\left[\left(\frac{\epsilon + r/2}{[\epsilon(\epsilon+r)]^{1/2}} - 1\right) - \frac{\beta^2 r^2(\epsilon + r/2)}{32[\epsilon(\epsilon+r)]^{5/2}}\right] , \tag{A2}$$

$$\sigma_{zz}^{\mathrm{DOS}} = -\frac{e^2 s r \kappa}{16\eta}\left[\ln\left(\frac{2}{\epsilon^{1/2} + (\epsilon+r)^{1/2}}\right)^2 - \frac{\beta^2(\epsilon + r/2)}{24[\epsilon(\epsilon+r)]^{3/2}}\right] , \tag{A3}$$

$$\sigma_{zz}^{\mathrm{MT(reg)}} = -\frac{e^2 s r \tilde{\kappa}}{16\eta}\left[\left(\frac{(\epsilon+r)^{1/2} - \epsilon^{1/2}}{r^{1/2}}\right)^2 - \frac{\beta^2 r}{48[\epsilon(\epsilon+r)]^{3/2}}\right] , \tag{A4}$$

and

$$\sigma_{zz}^{\mathrm{MT(an)}}=\frac{e^2 s}{16\eta}\left[\left[\frac{\epsilon+\gamma+r}{[\epsilon(\epsilon+r)]^{1/2}+[\gamma(\gamma+r)]^{1/2}}-1\right]-\frac{\beta^2 r^2(\epsilon+\gamma+r)\{\epsilon(\epsilon+r)+\gamma(\gamma+r)+[\epsilon(\epsilon+r)\gamma(\gamma+r)]^{1/2}\}}{96[\epsilon(\epsilon+r)\gamma(\gamma+r)]^{3/2}\{[\epsilon(\epsilon+r)]^{1/2}+[\gamma(\gamma+r)]^{1/2}\}}\right] . \tag{A5}$$

In (A3), we have assumed $\epsilon \ll 1$ and $\beta \ll 1$, as in (15).

Using (A2)–(A5), expression (31) for the position of the resistive maximum becomes modified to

$$\frac{\epsilon_m}{r}\approx\frac{1}{(8r\kappa)^{1/2}}\left[1-\frac{5\beta^2\kappa}{3r}\right]-\frac{\tilde{\kappa}}{8\kappa}+\frac{1}{16\gamma\kappa} . \tag{A6}$$

Note that the magnetic field reduces T_m by an amount proportional to B^2.

We now consider the "strong"-field regime $\epsilon_B \ll \beta \ll 1$. In this case, the sums over n in (37), (39), and (40) converge rapidly, and it suffices to keep only the $n=0$ term in the sums. For the DOS contribution, the formal logarithmic divergence of the sum requires that we treat (38) a bit differently. In this case, we separate out the $n=0$ term, and cut off the remaining sum at $n=n_{\max}\sim 1/\beta$. In this high-field limit, we clearly have $\gamma_B \gg \epsilon_B$. In most circumstances, the combined zero field and magnetic pair breaking present in $\gamma_B=\gamma+\beta/2$ is sufficiently strong that $r \ll \gamma_B$. Hence, we may approximate the anomalous MT term for $\gamma_B \gg \max(\epsilon_B, r)$. In this limit, the regular and anomalous MT terms are proportional to each other and may be combined. We find

$$\sigma_{zz}^{\mathrm{AL}}\approx\frac{e^2 s r^2\beta}{128\eta}\frac{1}{[\epsilon_B(\epsilon_B+r)]^{3/2}} , \tag{A7}$$

$$\sigma_{zz}^{\mathrm{DOS}}\approx-\frac{e^2 s r\kappa\beta}{16\eta}\left[\frac{1}{[\epsilon_B(\epsilon_B+r)]^{1/2}}+\ln\frac{1}{\beta}\right] , \tag{A8}$$

$$\sigma_{zz}^{\mathrm{MT}}\approx-\frac{e^2 s\beta}{8\eta}\left[\tilde{\kappa}-\frac{1}{2\gamma_B}\right]\left[\frac{\epsilon_B+r/2}{[\epsilon_B(\epsilon_B+r)]^{1/2}}-1\right] . \tag{A9}$$

Assuming the resistive maximum occurs in the 2D regime, we have

$$\frac{\epsilon_{Bm}}{r}\approx\left[\frac{3}{8r\kappa}\right]^{1/2}-\frac{\tilde{\kappa}}{2\kappa}+\frac{1}{4\gamma_B\kappa} . \tag{A10}$$

Note that (A10) is very similar to (A6), the leading term differing by $\sqrt{3}$, and the zero-field correction terms by a factor of 4. However, since both ϵ_{Bm} and γ_B depend *linearly* upon β, the magnetic field decreases T_m by an amount linear in B.

We now present the low-field expansions for the contributions to the fluctuation conductivity parallel to the layers. Using the Euler-Maclaurin approximation formula, we obtain

$$\sigma_{xx}^{\mathrm{AL}}=\frac{e^2}{16s}\left[\frac{1}{[\epsilon(\epsilon+r)]^{1/2}}-\frac{\beta^2[8\epsilon(\epsilon+r)+3r^2]}{32[\epsilon(\epsilon+r)]^{5/2}}\right] , \tag{A11}$$

$$\sigma_{xx}^{\mathrm{DOS}}+\sigma_{xx}^{\mathrm{MT(reg)}}=-\frac{e^2(\kappa+\tilde{\kappa})}{4s}\left[2\ln\left[\frac{2}{\epsilon^{1/2}+(\epsilon+r)^{1/2}}\right]-\frac{\beta^2(\epsilon+r/2)}{24[\epsilon(\epsilon+r)]^{3/2}}\right] , \tag{A12}$$

and

$$\sigma_{xx}^{\mathrm{MT(an)}}=\frac{e^2}{8s(\epsilon-\gamma)}\left[2\ln\left[\frac{\epsilon^{1/2}+(\epsilon+r)^{1/2}}{\gamma^{1/2}+(\gamma+r)^{1/2}}\right]-\frac{\beta^2}{24}\left[\frac{\gamma+r/2}{[\gamma(\gamma+r)]^{3/2}}-\frac{\epsilon+r/2}{[\epsilon(\epsilon+r)]^{3/2}}\right]\right] . \tag{A13}$$

The zero-field term in $\sigma_{xx}^{\mathrm{AL}}$ was first given by Lawrence and Doniach,[35] and the term of order β^2 was first obtained explicitly in Ref. 34, by inverting the order of the summation over n and the integration over q_z. Here we merely confirmed that it can be obtained from the full expression given in Ref. 3 using the Euler-Maclaurin formula. In addition, (A11) was given to order β^4 in Ref. 34. However, in our numerical calculations, we have used the full formulas (41)–(43), as was done for σ_{zz}, with the modifications mentioned in the text.

---

[1] S. Martin *et al.*, Phys. Rev. B **41**, 846 (1990); S. Martin *et al.*, Appl. Phys. Lett. **54**, 72 (1989).

[2] A. H. Thompson, F. R. Gamble, and R. F. Koehler, Jr., Phys. Rev. B **5**, 2811 (1972); A. H. Thompson, Solid State Commun. **13**, 1911 (1973).

[3] R. A. Klemm, J. Low Temp. Phys. **16**, 381 (1974); R. A. Klemm, Ph.D. thesis, Harvard University, 1974 (unpublished).

[4] T. A. Friedmann, M. W. Rabin, J. Giapintzakis, J. P. Rice, and D. M. Ginsberg, Phys. Rev. B **42**, 6217 (1990).

[5] M. Charalambous, J. Chaussy, and P. Lejay, Phys. Rev. B **45**, 5091 (1992).

[6] C. Baraduc, V. Pagnon, A. Buzdin, J. Y. Henry, and C. Ayache, Phys. Lett. A **166**, 267 (1992).

[7] G. Briceño, M. F. Crommie, and A. Zettl, Phys. Rev. Lett. **66**, 2164 (1991); Physica C **204**, 389 (1993).

[8] B. Veal (private communication); C. Ayache (private communication).

[9] L. B. Ioffe, A. I. Larkin, A. A. Varlamov, and L. Yu, Phys. Rev. B **47**, 8936 (1993).

[10] G. Balestrino, E. Milani, and A. Varlamov, Physica C **210**, 386 (1993); G. Balestrino, M. Marinelli, E. Milani, A. Varlamov, and L. Yu, Phys. Rev. B **47**, 6037 (1993).

[11] R. Ikeda, T. Ohmi, and T. Tsuneto, J. Phys. Soc. Jpn. **58**, 1377 (1989); **60**, 1051 (1991).

[12] S. Ullah and A. T. Dorsey, Phys. Rev. B **44**, 262 (1991).

[13] A. A. Varlamov and V. V. Dorin, Zh. Eksp. Teor. Fiz. **91**, 1955 (1986) [Sov. Phys. JETP **64**, 1159 (1986)].

[14] E. Abrahams, M. Redi, and J. W. Woo, Phys. Rev. B **1**, 208 (1970).

[15] C. DiCastro, C. Castellani, R. Raimondi, and A. Varlamov, Phys. Rev. B **42**, 10 211 (1990).

[16] K. E. Gray and D. H. Kim, Phys. Rev. Lett. **70**, 1693 (1993).

[17] A. Varlamov and V. Dorin, Zh. Eksp. Teor. Fiz. **84**, 1868 (1983) [Sov. Phys. JETP **57**, 1089 (1983)].

[18] A. Varlamov, V. Dorin, and I. Smolyarenko, Zh. Eksp. Teor. Fiz. **94**, 257 (1988) [Sov. Phys. JETP **67**, 2536 (1988)].

[19] R. A. Klemm and S. H. Liu, Phys. Rev. B **44**, 7526 (1991); **45**, 415 (1992).

[20] S. H. Liu and R. A. Klemm, Phys. Rev. B **48**, 4080 (1993).

[21] R. A. Klemm, M. R. Beasley, and A. Luther, Phys. Rev. B **8**, 5072 (1973); **12**, 877 (1975).

[22] A. Barone and G.-F. Paterno, *Physics and Applications of the Josephson Effect* (Wiley-Interscience, New York, 1981).

[23] G. Balestrino, A. Nigro, R. Vaglio, and M. Marinelli, Phys. Rev. B **39**, 12 275 (1989); G. Balestrino *et al.*, *ibid.* **46**, 14 919 (1992).

[24] J. B. Bieri and K. Maki, Phys. Rev. B **42**, 4854 (1990); J. B. Bieri, K. Maki, and R. S. Thompson, *ibid.* **44**, 4709 (1991).

[25] A. G. Aronov, S. Hikami, and A. I. Larkin, Phys. Rev. Lett. **62**, 965 (1989); **62**, 2336 (1989).

[26] R. A. Klemm and A. A. Varlamov (unpublished).

[27] L. G. Aslamazov and A. A. Varlamov, Zh. Eksp. Teor. Fiz. **77**, 2410 (1979) [Sov. Phys. JETP **50**, 1164 (1979)]; J. Low Temp. Phys. **38**, 223 (1980).

[28] L. P. Gor'kov, Zh. Eksp. Teor. Fiz. **36**, 1918 (1959) [Sov. Phys. JETP **9**, 1364 (1959)].

[29] R. A. Klemm, Phys. Rev. B **41**, 2073 (1990).

[30] L. Reggiani, R. Vaglio, and A. Varlamov, Phys. Rev. B **44**, 9541 (1991).

[31] B. L. Al'tshuler, M. Yu. Reyzer, and A. A. Varlamov, Zh. Eksp. Teor. Fiz. **84**, 2280 (1983) [Sov. Phys. JETP **57**, 1329 (1983)].

[32] H. Mikeska and H. Schmidt, Z. Phys. **230**, 239 (1970).

[33] K. Maki and R. S. Thompson, Phys. Rev. B **39**, 2767 (1989).

[34] S. Hikami and A. I. Larkin, Mod. Phys. Lett. B **2**, 693 (1988).

[35] W. E. Lawrence and S. Doniach, in *Proceedings of the Twelfth International Conference on Low Temperature Physics,* edited by E. Kanda (Academic of Japan, Kyoto, 1971), p. 361.

[36] R. A. Klemm (unpublished).

[37] M. J. Graf, D. Rainer, and J. A. Sauls (unpublished).

[38] A. F. Volkov, Pis'ma Zh. Teor. Fiz. **57**, 217 (1993) [JETP Lett. **57**, 226 (1993)].

[39] B. Al'tshuler (private communication).

[40] V. V. Dorin (unpublished).

[41] P. W. Anderson and Z. Zou, Phys. Rev. Lett. **60**, 132 (1988).

[42] D. Mandrus *et al.*, Phys. Rev. Lett. **70**, 2629 (1993).